Photoacoustics 38 (2024) 100606

Contents lists available at ScienceDirect

Photoacoustics

journal homepage: www.elsevier.com/locate/pacs

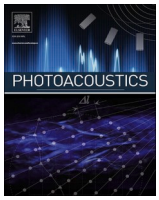

Optimizing breast cancer diagnosis with photoacoustic imaging: An analysis of intratumoral and peritumoral radiomics

Zhibin Huang [a,1], Sijie Mo [a,1], Huaiyu Wu [a,1], Yao Kong [a], Hui Luo [a], Guoqiu Li [a], Jing Zheng [a], Hongtian Tian [a], Shuzhen Tang [a], Zhijie Chen [c], Youping Wang [d], Jinfeng Xu [a,2], Luyao Zhou [b,2], Fajin Dong [a,*,2]

[a] Department of Ultrasound, The Second Clinical Medical College, Jinan University (Shenzhen People's Hospital), Shenzhen 518020, China
[b] Department of Ultrasound, Shenzhen Children' Hospital, No. 7019, Yitian Road, Futian District, Shenzhen 518026, China
[c] Ultrasound Imaging System Development Department, Shenzhen Mindray Bio-Medical Electronics Co., Ltd., Shenzhen, China
[d] Department of Clinical and Research, Shenzhen Mindray Bio-medical Electronics Co., Ltd., Shenzhen, China

ARTICLE INFO

Keywords:
Breast cancer
Photoacoustic imaging
Radiomics
Ultrasound
Prediction

ABSTRACT

Background: The differentiation between benign and malignant breast tumors extends beyond morphological structures to encompass functional alterations within the nodules. The combination of photoacoustic (PA) imaging and radiomics unveils functional insights and intricate details that are imperceptible to the naked eye.
Purpose: This study aims to assess the efficacy of PA imaging in breast cancer radiomics, focusing on the impact of peritumoral region size on radiomic model accuracy.
Materials and methods: From January 2022 to November 2023, data were collected from 358 patients with breast nodules, diagnosed via PA/US examination and classified as BI-RADS 3–5. The study used the largest lesion dimension in PA images to define the region of interest, expanded by 2 mm, 5 mm, and 8 mm, for extracting radiomic features. Techniques from statistics and machine learning were applied for feature selection, and logistic regression classifiers were used to build radiomic models. These models integrated both intratumoral and peritumoral data, with logistic regressions identifying key predictive features.
Results: The developed nomogram, combining 5 mm peritumoral data with intratumoral and clinical features, showed superior diagnostic performance, achieving an AUC of 0.950 in the training cohort and 0.899 in validation. This model outperformed those based solely on clinical features or other radiomic methods, with the 5 mm peritumoral region proving most effective in identifying malignant nodules.
Conclusion: This research demonstrates the significant potential of PA imaging in breast cancer radiomics, especially the advantage of integrating 5 mm peritumoral with intratumoral features. This approach not only surpasses models based on clinical data but also underscores the importance of comprehensive radiomic analysis in accurately characterizing breast nodules.

Summary

This study reveals that combining 5 mm peritumoral and intratumoral photoacoustic imaging features with clinical data markedly improves the accuracy of breast cancer diagnostics.

1. Introduction

Breast cancer (BC) remains the most frequently diagnosed cancer among women and constitutes a major cause of cancer-related mortality worldwide [1]. The critical role of early detection and intervention in

Abbreviations: BC, breast cancer; PA, Photoacoustic; US, ultrasound; ROI, region of interest; PA/US, Photoacoustic/ultrasound; GSUS, gray-scale US; MRI, magnetic resonance imaging; BI-RADS, Breast Imaging-Reporting and Data System; ROC, receiver operating characteristic curve; CI, confidence interval; AUC, area under the curve; IQR, interquartile range.

* Corresponding author.
E-mail addresses: zhouly6@mail.sysu.edu.cn (L. Zhou), dongfajin@szhospital.com (F. Dong).

[1] These authors contributed equally to this work.
[2] Co-senior Authors.

https://doi.org/10.1016/j.pacs.2024.100606
Received 24 January 2024; Received in revised form 26 March 2024; Accepted 5 April 2024
Available online 9 April 2024

improving survival rates and quality of life in BC patients is well-documented [2,3], particularly in asymptomatic women, where early diagnosis can significantly impact disease prognosis.

While ultrasound (US), mammography, and magnetic resonance imaging (MRI) are the primary non-invasive breast imaging modalities, each presents limitation. Mammography, although effective in detecting calcifications, shows reduced sensitivity in dense breast tissue, notably in Asian women [4,5]. MRI, despite its superior sensitivity, is hampered by high false-positive rates and several contraindications, limiting its applicability [6,7]. US, on the other hand, is non-invasive, cost-effective, and accessible, proving beneficial in early cancer detection when combined with mammography [8–10]. However, its limitations, including the lack of functional nodule information and morphological overlap, leading to increased false positives, necessitate enhanced precision in US assessments for BC [8,11].

Photoacoustic (PA) imaging, integrated with conventional US, offers a synergistic diagnostic approach to address these challenges. Combining laser and US technologies, photoacoustic/ultrasound (PA/US) imaging provides detailed morphological and functional insights, including tumor vasculature imaging and quantification of oxyhemoglobin and deoxyhemoglobin levels, enhancing diagnostic accuracy [12–15]. Despite these advancements, the differentiation of benign and malignant lesions in PA/US imaging often relies on subjective visual scoring methods.

Radiomics refers to a variety of computerized approaches that aimed to extract quantitative features from medical images including morphological features, intensity, texture and functional information, which are incredible to be recognized or quantifies by human eye [16]. Traditionally, radiomics mainly focused on the primary tumor, negligent of the peritumoral regions. However, different tumors have different tendency of invasion, and the peritumoral regions serves as the first path of tumor invasion, reflecting the complementary role of peritumoral regions in diagnosing tumors [17]. Recent studies demonstrated that the MRI feature of 0–8 mm region of interest (ROI) of peritumoral region in BC is associated with preoperative targeted therapy efficiency of BC [18]. However, little is known about the PA/US imaging features in the peritumoral regions of BC and identifying the peritumoral PA/US imaging features is of great significance in the diagnosis of BC.

In this study, we developed a nomogram model incorporating the clinic features, intratumoral and peritumoral radiomic features to predict the benign and malignant nature of BI RADS 3–5 breast nodules. Our results showed that the nomogram model has higher predicting efficiency of malignant breast nodules when comparing with the one using clinic features or radiomic features alone. Moreover, among the different peritumoral size, 5 mm-ROI of intratumoral and peritumoral region has the best predicting efficiency for the identification of malignant breast nodules, indicating that 5 mm-ROI of intratumoral and peritumoral PA imaging radiomics have potential diagnostic value in BI RADS 3–5 breast nodules.

2. Materials and methods

2.1. Statement of ethics

This study was executed in strict adherence to the principles outlined in the Declaration of Helsinki (2013 revision) and received approval from the Medical Ethics Committee of our hospital (Approval No. SYL-202161–02). All participants provided written informed consent.

2.2. Participants

This study encompassed a consecutive cohort of 358 patients in BI-RADS 3–5 breast nodules who underwent PA/US examinations and subsequent surgical interventions for breast lesions at our institution from January 2022 to November 2023. The pathological validation for benign lesions was acquired via 14-gauge core needle biopsies, whereas the confirmation of malignant tumors was based on postoperative pathological findings. The exclusion criteria were meticulously defined as follows:

(a) pregnant or lactating women; (b) individuals with compromised skin integrity in the assessment area (e.g., cuts, open wounds, ulcers); (c) patients with ongoing or active breast or axillary infections on the assessed side; (d) presence of subcutaneous congestion, hemorrhagic purpura, or nevus nigricans in the imaging area; (e) history of psychiatric disorders rendering the patient unable to comply with the testing protocol; (f) patients who had received neoadjuvant chemotherapy within three months prior to the examination; (g) cases with incomplete pathological records, a history of radiotherapy or chemotherapy, or suboptimal US image quality. Fig. 1 illustrates a flowchart delineating the patient inclusion process and Fig. 2 illustrates a Workflows for the necessary steps in radiomics model Construction.

2.3. Multimodal PA/US imaging system and examination

Multimodal PA/US examinations of all subjects were performed by a radiologist with 10 years of experience in breast US. The equipment used is the L9–3 linear array probe of Mindray Resona 7 (Mindray, China, refer to Appendix E1 for specific settings). A one-two bifurcated optical fiber bundle (Ceramoptec GmbH), which was mounted by a custom-made holder onto the both sides of the probe, was used to deliver the laser. The laser was emitted to tissues while the generated photoacoustic signals, which presented as the form of ultrasonic waves, were detected by the linear ultrasonic transducer. An OPO tunable laser (Spitlight 600-OPO, Innolas laser GmbH), which generated 680–980 nm laser pulses at 10 Hz, were utilized. In this study, 750 nm and 830 nm wavelengths were selected for PA imaging, at which the deoxygenated hemoglobin and oxygenated hemoglobin could reach the peak absorption respectively.

The imaging procedures were meticulously conducted under controlled environmental conditions with a temperature range of 20–25°C and humidity maintained between 50% and 70%. Prior to the examination, laser safety glasses were provided to both the operator and the patients to ensure compliance with safety protocols. Patients were positioned supinely for the examination, with adjustments made to other suitable positions as required by the scanning protocol. To facilitate comprehensive access to the breast and axillary regions, the affected arm was positioned in 180° abduction. The examination commenced with the identification of breast lesions via grayscale US. Following this, a US gel pad was placed on the skin overlying the lesion to optimize

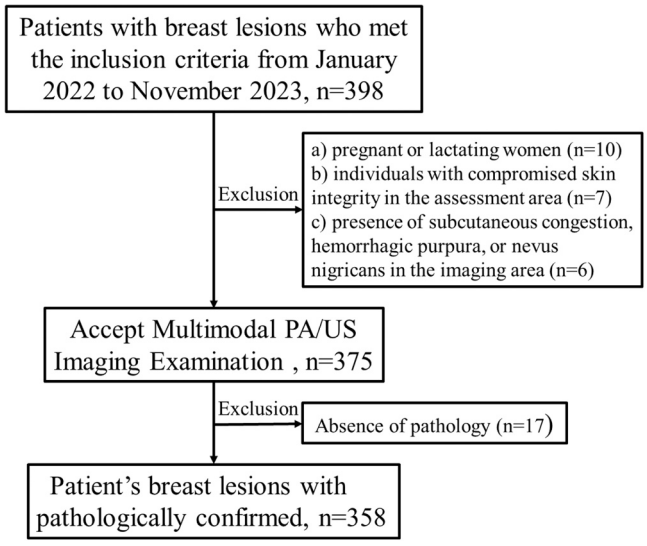

Fig. 1. : Flowchart of patient inclusion and exclusion criteria.

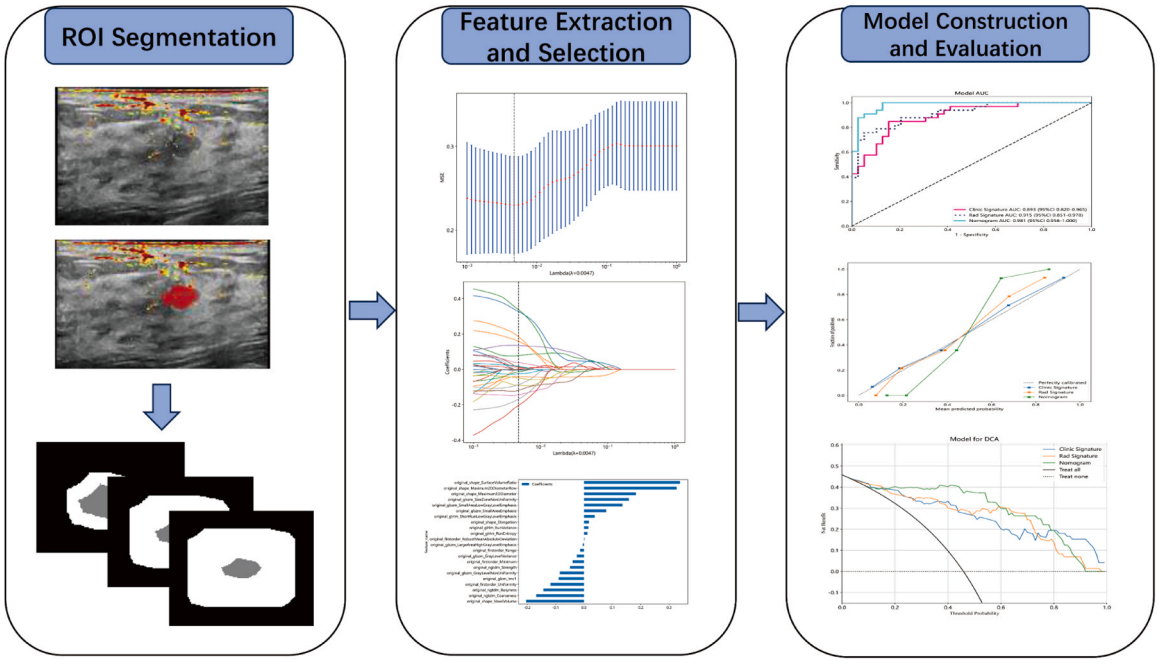

Fig. 2. : Workflows for the necessary steps in the current study. Manual segmentation of tumors is performed on ultrasound images, followed by automatic outward expansion of the tumor perimeter by 2 mm, 5 mm, and 8 mm, respectively. Imaging histological features are extracted from ultrasound images of different regions of interest (ROI) within and around the tumor to quantify characteristics such as tumor shape. For feature selection, ICC, Spearman correlation coefficient, and LASSO are used to select the extracted features. The performance of the predictive model is evaluated by the area under the receiver operating characteristic (ROC) curve. To provide more understandable measurement results, we developed a personalized nomogram evaluation tool that assesses the fit of the nomogram via calibration curves and analyzes the clinical utility of the nomogram through decision curves.

acoustic coupling. The probe, positioned on the gel pad, was meticulously aligned to ensure that the largest cross-sectional view of the lesion was centralized on the display screen. Stability of the image was a key focus, with the probe held steadily (Appendix E2). once a stable and clear image was achieved, it was saved in the system for subsequent analysis. In the multimodal mode, the real-time imaging screen was divided into four segments. The top-left quadrant presented a standard US image, permitting the selection of grayscale ultrasound (GSUS), color Doppler US, or Power Doppler US. The bottom two quadrants displayed photoacoustic images superimposed on GSUS images at wavelengths of

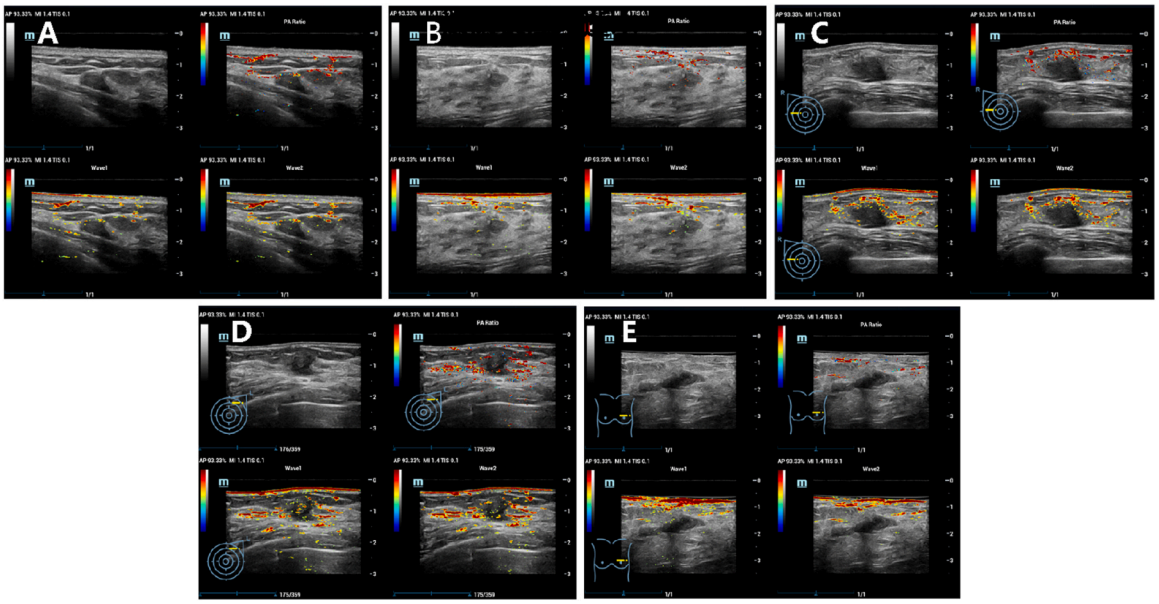

Fig. 3. : Photoacoustic/ultrasound (PA/US) image of benign lesion or malignant lesion. Note: A: PA/US image of benign lesion (BI-RADS 3, Fibroadenoma); B: PA/US image of benign lesion (BI-RADS 4 A, Intraductal papilloma); C: PA/US image of malignant lesion (BI-RADS 4B, Invasive non-special type carcinoma); D: PA/US image of malignant lesion (BI-RADS 4 C, Invasive non-special type carcinoma); E: PA/US image of malignant lesion (BI-RADS 5, Invasive non-special type carcinoma). In the multimodal mode, the real-time imaging screen was divided into four segments. The top-left quadrant presented a standard US image, permitting the selection of grayscale ultrasound (GSUS), color Doppler US, or Power Doppler US. The bottom two quadrants displayed photoacoustic images superimposed on GSUS images at wavelengths of 750 nm (Wave 1) and 830 nm (Wave 2), respectively. The top-right quadrant showcased oxygen saturation (So2) mapping in pseudocolor, representing oxygenation derived from the combined signals of the two photoacoustic images at 750 nm and 830 nm.

750 nm and 830 nm, respectively. The top-right quadrant showcased oxygen saturation (So_2) mapping in pseudocolor, representing oxygenation derived from the combined signals of the two photoacoustic images at 750 nm and 830 nm (Fig. 3).

2.4. Region-of-interest segmentation and radiation feature extraction

For the analysis, a singular image per tumor was employed. All PA images in the study were archived in the Digital Imaging and Communications in Medicine (DICOM) format. The ROI for feature extraction was manually delineated on the largest cross-sectional area of the PA image using ITK-SNAP software (version 3.8.0; [http://www.itksnap.org]). This task was undertaken by two seasoned breast radiologists, each boasting over a decade of expertise in breast US, who were unaware of the final pathological outcomes. Intraclass correlation coefficients (ICC) were calculated using 60 randomly selected PA images to assess the reliability and reproducibility of the features (Appendix E3). Radiomic features demonstrating an ICC greater than 0.75, indicative of excellent stability, were selected for feature extraction [19]. Standardization of feature lines was accomplished via z-score normalization, and feature correlations were assessed using the Spearman correlation coefficient. In instances where the correlation coefficient exceeded 0.9, only one of the correlated features was retained. Additionally, a Mann-Whitney test was performed on the features and any feature with a P value greater than 0.05 was eliminated. In this study, the construction of radiomic features was facilitated using the least absolute shrinkage and selection operator (LASSO) regression model, applied to the training dataset. The LASSO methodology effectively diminishes regression coefficients towards zero, consequently assigning zero coefficients to numerous non-essential features, contingent on the weighting parameter λ. The optimal λ was determined through a 10-fold cross-validation process, employing a minimum criterion approach. This method identified the λ value that resulted in the minimal cross-validation error. Subsequently, the parameters of the retained features with non-zero coefficients were incorporated into the regression model fitting. The Pyradiomics platform (https://pyradiomics.readthedocs.io/en/latest/index.html) was utilized for automated extraction of these radiomic features from each image[20].

2.5. Establishment performance and validation of the radiodiomic model

A LASSO regression model was employed to construct a predictive model for distinguishing between benign and malignant breast lesions within the training cohort. The model's diagnostic efficacy was assessed using indices such as accuracy, sensitivity, and specificity, all derived from the confusion matrix and their respective derivations. Additionally, univariate logistic regression analysis was conducted to identify independent predictors of benign and malignant breast nodules. This analysis encompassed variables such as age, menopausal status, radiomics characteristics, the diameter of the lesion as reported by US. Subsequently, a radiomics nomogram integrating these radiomics characteristics and independent prognostic factors was developed. The diagnostic utility of this radiomics nomogram was then validated in a separate cohort, with its performance evaluated through the construction of a Receiver Operating Characteristic (ROC) curve. To assess the calibration efficacy of the nomogram, a calibration curve was plotted, and the Hosmer-Lemeshow test was utilized to evaluate its calibration accuracy. Furthermore, a Decision Curve Analysis (DCA) was performed to determine the clinical utility of the predictive model (Fig. 2).

2.6. Statistical analysis

Statistical analysis was performed using R 4.2.2(Copyright (C) 2022 The R Foundation for Statistical Computing). A two-sided p-value threshold of less than 0.05 was established as the criterion for statistical significance. During the univariate analysis, the clinical characteristics of patients across different groups were compared. For continuous variables, the Mann–Whitney U test was employed, while categorical variables were analyzed using either the $\chi 2$ test or Fisher's exact test, contingent upon the appropriateness to the data set. Additionally, for comparisons involving more than two groups, Analysis of Variance (ANOVA) and the Kruskal–Wallis H test was utilized.

3. Results

3.1. Patient clinical outcomes

A total of 358 cases of BI-RADS 3–5 breast nodule patients were divided into two groups, with 286 patients in the training set and 72 patients in the testing set. The pathological results showed 156 benign nodules and 130 malignant nodules in the training set, 39 benign nodules and 33 malignant nodules in the testing set. The clinical features of these patients were summarized in Table 1 and Table S1 concerning the age, height, weight, diameter, location, which showed no significant difference among these characteristics between the training set and testing set ($P>0.05$). Univariate analysis showed that weight, the maximum of the nodule, the minimum of the nodule, age and menstruation stage were significantly associated with the malignancy of breast nodules ($P<0.001$). Multivariate analysis revealed significant correlation between the maximum of the nodule, the minimum of the nodule and age ($P<0.001$) (Table 2), which were selected for further model construction. In the development of our clinical model, we incorporated age and tumor diameter as primary variables. This model demonstrated robust discriminating ability with an Area Under the Curve (AUC) of 0.863 (95% Confidence Interval [CI]: 0.819–0.907) in the training dataset. Notably, this high level of discrimination was consistent in the test dataset, where the model achieved an AUC of 0.794 (95% CI: 0.710–0.878) (Figure S1).

3.2. Intratumoral and peritumoral feature selection and ultrasound radiomic model construction

Within the tumor and at peritumoral regions of 2 mm, 5 mm, and 8 mm ROI, we extracted a total of 214 radiomic features (The specific feature distribution and weights are detailed in Figure S2-S5). These included 107 intratumoral features and 107 peritumoral features. From the filtered set of 107 intratumoral and 107 peritumoral features, 35 optimal intratumoral features were selected using LASSO regression for inclusion in the intratumoral PA imaging radiomics model (Fig. 4A). Additionally, 37 optimal features combining intratumoral and 2 mm peritumoral (Fig. 4B), 33 combining intratumoral and 5 mm peritumoral (Fig. 4C), and 32 combining intratumoral and 8 mm peritumoral features (Fig. 4D) were incorporated to establish distinct combined intratumoral-peritumoral PA imaging radiomics models. The results showed that the intratumoral PA imaging radiomic model had an AUC of 0.842 (95% CI: 0.794–0.891) in the training set and 0.745 (95% CI: 0.648–0.841) in the testing set (Fig. 4E). While in the intratumor combined the 2 mm-ROI of peritumor PA imaging radiomics model and clinical model, the features had an AUC of 0.885 (95% CI: 0.845–0.925) in the training set (Fig. 4F) and an AUC of 0.826 (95% CI: 0.743–0.910) in the testing set (Fig. 4G). In the intratumor combined the 5 mm-ROI of peritumor PA imaging radiomics model and clinical model, the results showed an AUC of 0.924 (95% CI: 0.892–0.957) in the training set (Fig. 4H) and an AUC of 0.873 (95% CI: 0.801–0.945) in the testing set (Fig. 4I). In the intratumor combined the 8 mm-ROI of peritumor PA imaging radiomics model and clinical model, the features showed an AUC of 0.903 (95% CI: 0.866–0.939) in the training set (Fig. 4J) and an AUC of 0.845 (95% CI: 0.823–0.945) in the testing set (Fig. 4K). The above results showed that incorporating peritumoral into radiomic analysis had better predicting performance than using intratumoral alone. Moreover, comparing the results of different peritumoral size revealed that peritumoral regions with 5 mm ROI has the best prediction

Table 1
Clinical characteristics of patients with breast nodules in training and testing sets (n=358).

Clinical feature	Training set				Testing set			
	ALL	Benign	Malignant	P value	ALL	Benign	Malignant	P value
Year	44.33±11.57	39.35±9.86	50.29±10.64	<0.001	44.29±11.62	39.77±10.83	49.64±10.28	<0.001
Height	159.49±5.55	159.72±6.25	159.22±4.58	0.63	159.85±5.16	160.19±5.54	159.45±4.72	0.39
Weight	58.15±7.76	56.48±6.73	60.16±8.45	<0.001	57.18±7.94	57.60±6.94	56.68±9.07	0.48
Max	19.69±12.14	16.65±9.09	23.34±14.21	<0.001	20.52±14.05	14.95±6.71	27.09±17.39	<0.001
Min	10.89±5.55	9.26±5.22	12.85±5.32	<0.001	10.97±6.02	8.35±4.83	14.08±5.86	<0.001
Menstruation				<0.001				0.01
No	198(69.23)	133(85.26)	65(50.00)		49(68.06)	32(82.05)	17(51.52)	
Yes	88(30.77)	23(14.74)	65(50.00)		23(31.94)	7(17.95)	16(48.48)	
Location				0.97				1.00
Right	151(52.80)	83(53.21)	68(52.31)		36(50.00)	19(48.72)	17(51.52)	
Left	135(47.20)	73(46.79)	62(47.69)		36(50.00)	20(51.28)	16(48.48)	

Note: Max = Maximum diameter; Min = Minimum diameter.

Table 2
Univariable and Multivariable analyses of the clinical charateristics and clinicopathologic features in patients in the training set (n=286).

	Univariable Analysis		Multivariable Analysis	
Variable	Log (OR)	p_value	Log (OR)	p_value
Year	1.02	<0.001	1.019	<0.001
Height	0.996	0.348	…	…
Weight	1.011	0.001	1	0.925
Max	1.012	<0.001	1.009	0.003
Min	1.032	<0.001	1.018	0.001
Menstruation	1.488	<0.001	0.918	0.29
Location	1.002	0.976	…	…

Note: OR=odds ratio, Max = maximum diameter; Min = minimum diameter.

performance. Detailed radiomics performance is shown in Table 3.

3.3. Combined model construction

In this study, we developed a comprehensive predictive model by integrating radiomics features derived from intratumoral and peritumoral 5 mm PA imaging with clinical risk factors. This model culminated in the creation of a nomogram, illustrated in Fig. 5 A, aimed at differentiating benign from malignant breast nodules within the BI-RADS 3–5 category. The model's performance was evaluated in terms of its AUC values. In the training set, the model achieved an AUC of 0.950 (95% CI: 0.925–0.975) (Fig. 4H), while in the test set, the AUC was 0.899 (95% CI: 0.841–0.956) (Fig. 4I). Additionally, the calibration curves for the combined intratumoral and 5 mm peritumoral PA imaging features with clinical parameters, demonstrate good calibration in both the training and test sets (Fig. 5B and C). The DCA showed that the nomogram incorporating the clinic features, intratumoral and 5 mm peritumoral PA imaging radiomic features had significant benefit for intervention in BI-RADS 3–5 breast nodules (Fig. 5D and E). The results of this study underscore the exceptional diagnostic capability of this nomogram, which integrates radiomic features based on photoacoustic imaging within the intratumoral and peritumoral 5 mm areas with clinical risk factors. This model demonstrates a high level of accuracy in differentiating between benign and malignant breast nodules, suggesting its utility in substantially reducing the need for unnecessary breast nodule biopsies.

4. Discussion

Prior studies have highlighted the potential of PA imaging in accurately diagnosing BC [12,14,15,21]. However, current diagnostic approaches predominantly rely on subjective image visualization scoring, with a notable absence of quantitative, non-invasive methodologies. Furthermore, there is a lack of comprehensive analysis regarding the imaging characteristics of breast nodules as depicted by photoacoustic imaging. Addressing these gaps, our study leveraged photoacoustic imaging, an innovative technology based on laser-generated US, for the non-invasive evaluation of breast nodules in participants. We aimed to elucidate the correlation between diverse regional radiomic signatures, as identified through photoacoustic imaging, and the benign or malignant nature of breast nodules. Crucially, this research culminated in the development and validation of a radiomics nomogram. This nomogram, integrating intratumoral radiomics features within a 5 mm peritumoral area, the diameter of the largest lesion section as reported by US, and patient age, proved effective in non-invasively predicting the benign or malignant status of BC patients' pre-surgery. In the context of non-invasively predicting the benign or malignant status of BC patients prior to surgery, the developed nomogram demonstrated significant diagnostic differentiation, evidenced by an Area Under the Curve (AUC) of 0.950 in the training cohort and 0.899 in the validation cohort. Notably, this model outperformed both the pure clinical feature model and the radiomics models of the intratumoral area combined with peritumoral 2 mm and 8 mm areas.

PA imaging has evolved from preclinical investigations on phantoms and animal models to clinical applications [14,22–24]. Optoacoustic device that generates temporally interleaved, coregistered, real-time images of grayscale US with fused color-coded optoacoustic features of benign and malignant breast nodules. The device's capability to fuse these distinct imaging modalities provides a comprehensive and detailed representation of the nodules, thereby facilitating more accurate and efficient diagnostic evaluations. Despite these advancements, the diagnostic process remains largely subjective, relying on the interpreting physician's expertise. This subjectivity underscores the inherent limitations of human visual assessment in detecting complex biological information present in medical images. To address this, radiomics emerges as a pivotal tool, enabling the extraction of objective, quantitative features from medical images through high-throughput computing [25,26]. This approach quantifies aspects such as tumor heterogeneity, offering valuable insights for tumor characterization and aiding in diagnostic and therapeutic decision-making [27]. In related studies, the efficacy of radiomics models in breast nodule diagnosis has been demonstrated. Hong et al.[28] achieved an AUC of 0.89 in diagnosing BI-RADS category 4–5 breast nodules. Romeo et al.[29] combined radiomics with machine learning to attain an AUC of 0.82, while Zhang et al.[30] developed an intratumoral radiomics model for Breast Imaging Reporting and Data System categories 3–5 nodules, yielding an AUC of 0.79 in their test set. In this study, employing LASSO regression, we identified and incorporated 36 intratumoral radiomics features into a photoacoustic radiomics model. This model demonstrated AUC values of 0.800 (95% CI: 0.739–0.855) and 0.780 (95% CI: 0.6854–0.875) in the training and test sets, respectively. While these values are slightly lower than those reported in the studies by Hong et al. [28], Romeo et al. [29] and Zhong et al. [30], they affirm the potential of integrating radiomics in PA imaging for breast nodule diagnosis.

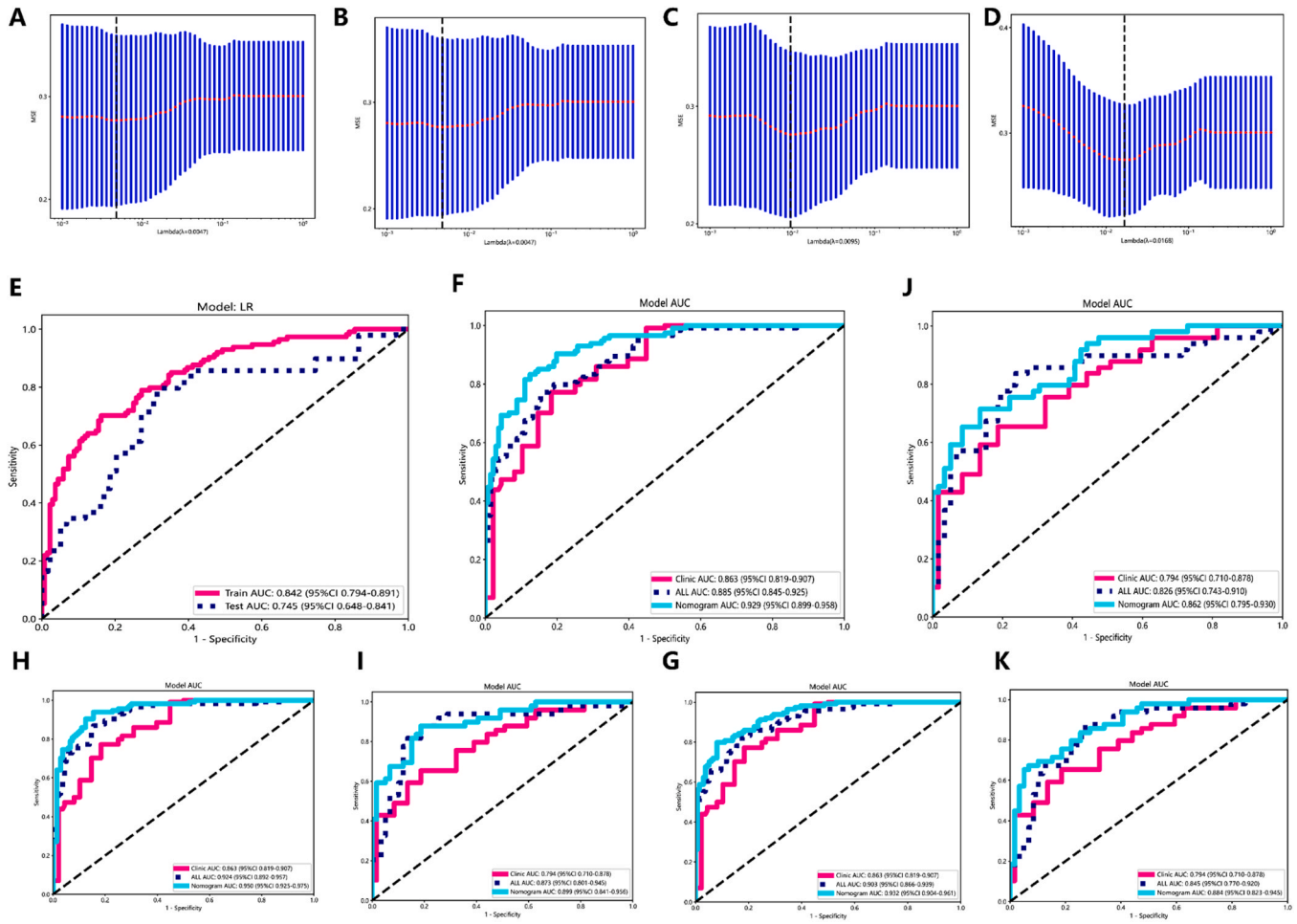

Fig. 4. : The AUC curves of the radiomic models in intratumoral and peritumoral regions. A. Radiomic features selected by LASSO in the intratumoral region. B-D. Radiomic features selected by LASSO in the intratumoral and 2 mm peritumoral region (B), intratumoral and 5 mm peritumoral region (C), intratumoral and 8 mm peritumoral region (D). E. AUC curves of image only radiomic models in the training and testing set. F and G. AUC curves of the clinic model, radiomic model and nomogram model in the training set (F) and testing set (G) of intratumoral and 2 mm peritumoral region. H and I. AUC curves of the clinic model, radiomic model and nomogram model in the training set (H) and testing set (I) of intratumoral and 5 mm peritumoral region. J and K. AUC curves of the clinic model, radiomic model and nomogram model in the training set (J) and testing set (K) of intratumoral and 8 mm peritumoral region.

Table 3
Diagnostic performance of radiomics model.

Model	Set	AUC	95% CI	Sensitivity	Specificity	Accuracy
Intra-radiomics	Training	0.842	0.794–0.891	0.809	0.632	0.728
	Testing	0.745	0.648–0.841	0.712	0.531	0.630
Intra+2 mm	Training	0.885	0.845–0.925	0.816	0.790	0.804
peri-radiomics+clinical	Testing	0.826	0.743–0.910	0.797	0.776	0.787
Intra+5 mm	Training	0.924	0.892–0.957	0.853	0.825	0.844
peri-radiomics+clinical	Testing	0.873	0.801–0.945	0.824	0.816	0.815
Intra+8 mm	Training	0.903	0.866–0.939	0.846	0.791	0.816
peri-radiomics+clinical	Testing	0.845	0.823–0.945	0.746	0.816	0.778

Note: AUC, area under the curve; CI: confidence interval; intra, intratumoral features; peri, peritumoral features.

Prior studies focused on the predictive role of intratumoral radiomic features, neglect of peritumoral regions[31–33]. However, as the development of biomedicine, researchers found that peritumoral tissues were also closely associated with tumor progression and prognosis, which raised a frenzied expansion of studying into peritumoral radiomics[34,35]. These studies mainly concerned on the MRI radiomic features of peritumoral regions and they found that peritumoral MRI radiomics have significant predictive value for the recurrence, chemotherapy response and survival time of BC patients[36]. However, there has been a limited investigation into the impact of radiomic features from US imaging of different peritumoral regions in the diagnosis and prognosis of BC. More significantly, to the best of our knowledge, the application of PA imaging as an emerging technique has not yet been explored for its potential in discerning radiomic features of the tumor and its adjacent areas in the diagnosis of breast lesions. In this study, we incorporated both intratumoral and peritumoral PA imaging radiomics to discriminate benign and malignant breast nodules, and we found the combined model had an AUC of 0.873 (95% CI: 0.801–0.945) in the testing set, much higher than using the intratumoral US radiomics alone, which was 0.745 (95% CI: 0.648–0.841). This may be attributed to the

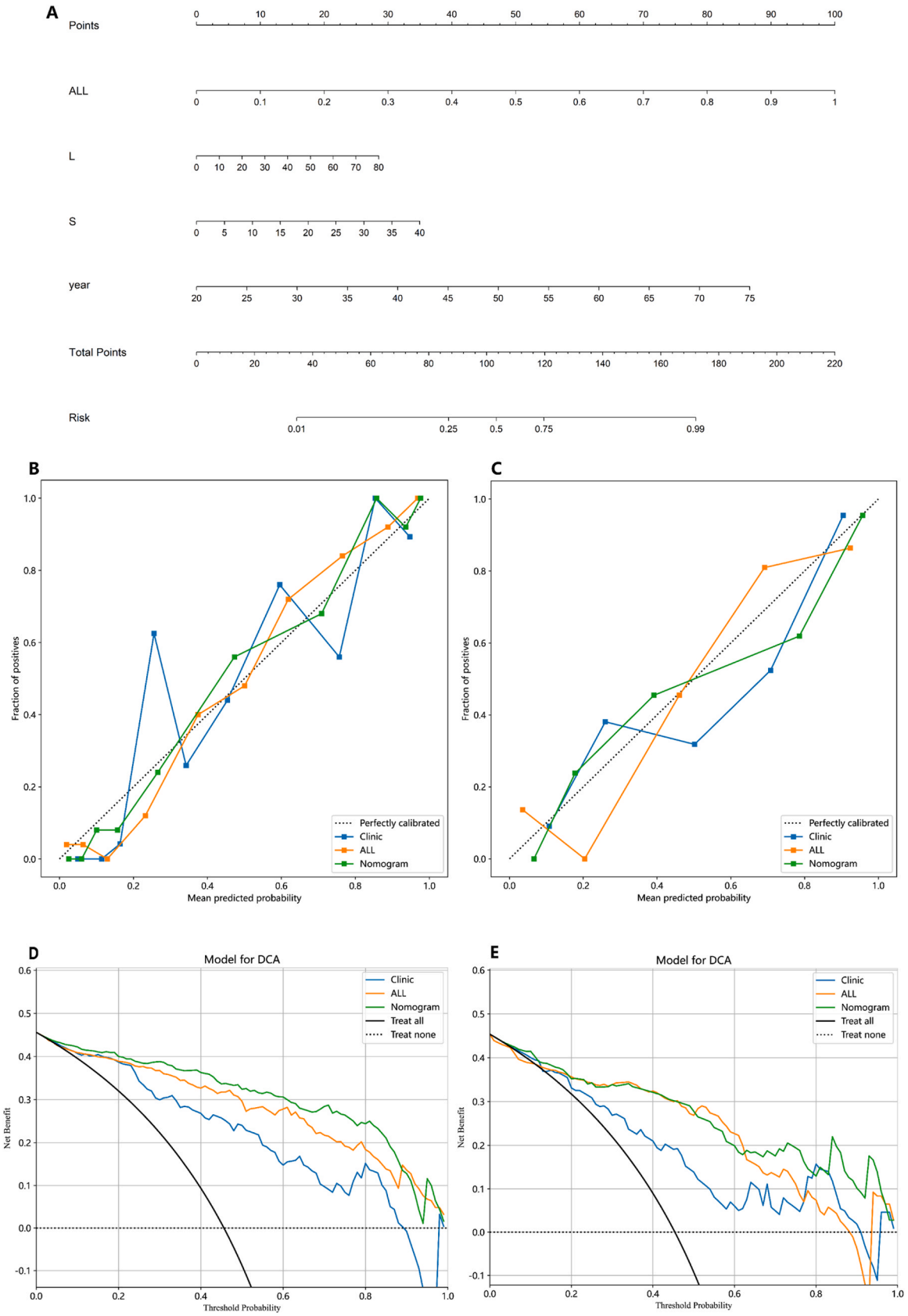

Fig. 5. The construction of nomogram model. A. A nomogram was developed incorporating the clinical features, intratumoral and peritumoral radiomic features. B and C. The calibration curves of the clinical model, radiomic model and nomogram model in the training (B) and testing sets (C). D and E. The decision curves of clinical model, radiomic model and nomogram model in the training (D) and testing sets (E).

fact that some BI-RADS 3–5 category nodules are challenging to identify solely based on intratumoral radiomic features, but can be discerned through peritumoral radiomic characteristics. Therefore, peritumoral radiomic features could potentially provide valuable assistance in cases where intratumoral radiomic features alone fall short of enabling accurate differentiation.

In this study, we explored the optimal peritumoral size by dividing the peritumoral region into 2 mm, 5 mm and 8 mm ROI. The results showed that 5 mm ROI has the highest AUC among these three categories, with an AUC of 0.826 (95% CI: 0.743–0.910) in the testing set of 2 mm ROI, 0.873 (95% CI: 0.801–0.945) of 5 mm ROI and 0.845 (95% CI: 0.823–0.945) of 8 mm ROI. To better define the predictive value of US radiomics in the benign and malignant features of breast nodules, we developed a nomogram model with the clinic features, intratumoral and 5 mm ROI peritumoral radiomics. The model showed an AUC was 0.899 (95% CI: 0.841–0.956) in the testing set. Our study revealed that peritumoral regions were crucial for benign and malignant breast nodule differentiation and 5 mm ROI of peritumoral region was the most optimal size. This finding is consistent with previous studies[30]. This may be for several reasons: Firstly, the 8 mm peritumoral region might be too expansive, including more normal breast tissue relative to a 5 mm margin, which does not contribute beneficially to radiomic analysis. Conversely, a 2 mm margin may fail to encompass sufficient breast tissue affected by invasion, offering less comprehensive information for radiomic analysis. Additionally, this might also be related to the field of view and sensitivity of the imaging probe. Previous research has shown that ultrasound images obtained by probes with different frequencies will affect the diagnostic performance of artificial intelligence models [37]. Radiomic analysis is reliant on the image features extracted, and the frequency of the probe could potentially influence outcomes. In summary, our findings not only validate the utility of peritumoral characteristics in radiomics but also indicate that the choice of peritumoral region size significantly influences the predictive outcomes of radiomic analyses. We propose that instead of employing arbitrary or indeterminate sizes of peritumoral regions—a common practice in most current radiomics studies—systematic comparisons to identify the optimal peritumoral thickness could substantially enhance predictive models and optimize their performance.

This study has several limitations. The first limitation was the single-center retrospective study with small sample, which may lead to bias. Larger dataset from multi-center needs to be added to improve the diagnostic accuracy of our model. The second limitation was that we did not incorporate two-dimensional ultrasonographic features in this model, which include shape, boundary, edges, internal echoes, posterior echoes and blood flow. These features were crucial for the differentiating of benign and malignant breast nodules. In the future, we will add these characteristics into our predictive model. Finally, in our study, the peritumoral radiomic features was only applied for the predicting of benign and malignant nodules. Whereas, the lymph node metastatic status, molecular subtypes, chemotherapy response and recurrence rate were also important prognostic factors of BC. Future work would validate the optimal peritumoral size dependent on different specific applications.

5. Conclusion

This study represents the first exploration into the utility of intratumoral and peritumoral features based on photoacoustic imaging in cancer radiomics analysis. Our findings corroborate that peritumoral features encompass critical information about the tumor itself, warranting their inclusion in future radiomics research. Furthermore, this work pioneers a systematic investigation of the impact of peritumoral region size in photoacoustic imaging-based cancer radiomics. Given that the selection of peritumoral size significantly influences the predictive accuracy of radiomics models, our study underscores the need to optimize peritumoral features in future radiomics investigations, thereby enhancing the overall predictive performance.

Ethics approval and consent to participate

This study was approved by the Institutional Review Board of the Shenzhen People's Hospital, specifically the Medical Ethics Committee of Shenzhen People 's Hospital. and all participants provided written informed consent. All methods were carried out in accordance with relevant guidelines and regulations.

Financial support

No.

CRediT authorship contribution statement

Jing Zheng: Resources, Data curation. **Hongtian Tian:** Project administration. **Guoqiu Li:** Methodology. **Luyao Zhou:** Writing – review & editing, Validation, Supervision. **Fajin Dong:** Writing – review & editing, Validation, Supervision. **Zhibin Huang:** Writing – original draft, Investigation, Data curation. **Shuzhen Tang:** Data curation. **Jinfeng Xu:** Writing – review & editing, Visualization, Validation. **Yao Kong:** Data curation. **Hui Luo:** Data curation. **Zhijie Chen:** Data curation, Methodology. **Sijie Mo:** Data curation. **Youping Wang:** Methodology. **Huaiyu Wu:** Investigation, Data curation, Conceptualization.

Declaration of Competing Interest

The authors declare that they have no known competing financial interests or personal relationships that could have appeared to influence the work reported in this paper

Data Availability

Data will be made available on request.

Acknowledgments

This work was supported by the National Key R&D Program of China (2023YFC2411700, 2023YFC2411705), Clinical Scientist Training Program of Shenzhen People's Hospital (SYWGSCGZH202202).

Appendix A. Supporting information

Supplementary data associated with this article can be found in the online version at doi:10.1016/j.pacs.2024.100606.

References

[1] A.N. Giaquinto, H. Sung, K.D. Miller, J.L. Kramer, L.A. Newman, A. Minihan, A. Jemal, R.L. Siegel, Breast cancer statistics, 2022, CA Cancer J. Clin. 72 (6) (2022) 524–541.
[2] P. Boyle, Global summit on mammographic screening, Ann. Oncol. 14 (8) (2003) 1159–1160.
[3] Force* UPST, Screening for breast cancer: recommendations and rationale, Ann. Intern. Med. 137 (5_Part_1) (2002) 344–346.
[4] R.W. Pinsky, M.A. Helvie, Mammographic breast density: effect on imaging and breast cancer risk, J. Natl. Compr. Cancer Netw. 8 (10) (2010) 1157–1165.
[5] K. Johnson, K. Lång, D.M. Ikeda, A. Åkesson, I. Andersson, S. Zackrisson, Interval breast cancer rates and tumor characteristics in the prospective population-based Malmö Breast Tomosynthesis Screening Trial, RADIOLOGY 299 (3) (2021) 559–567.
[6] C.K. Kuhl, A. Keulers, K. Strobel, H. Schneider, N. Gaisa, S. Schrading, Not all false positive diagnoses are equal: on the prognostic implications of false-positive diagnoses made in breast MRI versus in mammography/digital tomosynthesis screening, Breast Cancer Res. 20 (1) (2018) 1–9.
[7] D. Saslow, C. Boetes, W. Burke, S. Harms, M.O. Leach, C.D. Lehman, E. Morris, E. Pisano, M. Schnall, S. Sener, American Cancer Society guidelines for breast screening with MRI as an adjunct to mammography, CA: Cancer J. Clin. 57 (2) (2007) 75–89.

[8] W.A. Berg, Z. Zhang, D. Lehrer, R.A. Jong, E.D. Pisano, R.G. Barr, M. Böhm-Vélez, M.C. Mahoney, W.P. Evans, L.H. Larsen, Detection of breast cancer with addition of annual screening ultrasound or a single screening MRI to mammography in women with elevated breast cancer risk, Jama 307 (13) (2012) 1394–1404.
[9] N. Ohuchi, A. Suzuki, T. Sobue, M. Kawai, S. Yamamoto, Y.-F. Zheng, Y.N. Shiono, H. Saito, S. Kuriyama, E. Tohno, Sensitivity and specificity of mammography and adjunctive ultrasonography to screen for breast cancer in the Japan Strategic Anti-cancer Randomized Trial (J-START): a randomised controlled trial, Lancet 387 (10016) (2016) 341–348.
[10] A.S. Tagliafico, M. Calabrese, G. Mariscotti, M. Durando, S. Tosto, F. Monetti, S. Airalda, B. Bignotti, J. Nori, A. Bagni, Adjunct screening with tomosynthesis or ultrasound in women with mammography-negative dense breasts: interim report of a prospective comparative trial, J. Clin. Oncol. (2016).
[11] A. Vlahiotis, B. Griffin, A.T. Stavros, J. Margolis, Analysis of utilization patterns and associated costs of the breast imaging and diagnostic procedures after screening mammography, Clin. Outcomes Res.: CEOR 10 (2018) 157–167.
[12] E.I. Neuschler, R. Butler, C.A. Young, L.D. Barke, M.L. Bertrand, M. Böhm-Vélez, S. Destounis, P. Donlan, S.R. Grobmyer, J. Katzen, et al., A pivotal study of optoacoustic imaging to diagnose benign and malignant breast masses: a new evaluation tool for radiologists, Radiology 287 (2) (2018) 398–412.
[13] G.L.G. Menezes, R.M. Pijnappel, C. Meeuwis, R. Bisschops, J. Veltman, P.T. Lavin, M.J. van de Vijver, R.M. Mann, Downgrading of breast masses suspicious for cancer by using optoacoustic breast imaging, RadiologY 288 (2) (2018) 355–365.
[14] Q. Zhu, A. Ricci, P. Hegde, M. Kane, E. Cronin, A. Merkulov, Y. Xu, B. Tavakoli, S. Tannenbaum, Assessment of functional differences in malignant and benign breast lesions and improvement of diagnostic accuracy by using US-guided diffuse optical tomography in conjunction with conventional US, Radiology 280 (2) (2016) 387–397.
[15] Q. Zhu, E.B. Cronin, A.A. Currier, H.S. Vine, M. Huang, N. Chen, C. Xu, Benign versus malignant breast masses: optical differentiation with US-guided optical imaging reconstruction, Radiology 237 (1) (2005) 57–66.
[16] M.E. Mayerhoefer, A. Materka, G. Langs, I. Haggstrom, P. Szczypinski, P. Gibbs, G. Cook, Introduction to radiomics, J. Nucl. Med. 61 (4) (2020) 488–495.
[17] R. Li, Peritumoral radiomics and predicting treatment response, JAMA Netw. Open 3 (9) (2020) e2016125.
[18] N. Braman, P. Prasanna, J. Whitney, S. Singh, N. Beig, M. Etesami, D.D.B. Bates, K. Gallagher, B.N. Bloch, M. Vulchi, et al., Association of peritumoral radiomics with tumor biology and pathologic response to preoperative targeted therapy for HER2 (ERBB2)-positive breast cancer, JAMA Netw. Open 2 (4) (2019) e192561.
[19] M. Nijiati, D. Aihaiti, A. Huojia, A. Abulizi, S. Mutailifu, N. Rouzi, G. Dai, P. Maimaiti, MRI-based radiomics for preoperative prediction of lymphovascular invasion in patients with invasive breast cancer, Front. Oncol. 12 (2022) 876624.
[20] T.V. Bartolotta, A.A.M. Orlando, M. Dimarco, C. Zarcaro, F. Ferraro, A. Cirino, D. Matranga, S. Vieni, D. Cabibi, Diagnostic performance of 2D-shear wave elastography in the diagnosis of breast cancer: a clinical appraisal of cutoff values, La Radiol. Med. 127 (11) (2022) 1209–1220.
[21] Q. Zhu, P.U. Hegde, A. Ricci, M. Kane, E.B. Cronin, Y. Ardeshirpour, C. Xu, A. Aguirre, S.H. Kurtzman, P.J. Deckers, et al., Early-stage invasive breast cancers: potential role of optical tomography with US localization in assisting diagnosis, Radiology 256 (2) (2010) 367–378.
[22] J. Menke, Photoacoustic breast tomography prototypes with reported human applications, Eur. Radiol. 25 (8) (2015) 2205–2213.
[23] K.S. Valluru, K.E. Wilson, J.K. Willmann, Photoacoustic imaging in oncology: translational preclinical and early clinical experience, Radiology 280 (2) (2016) 332–349.
[24] Y. Goh, G. Balasundaram, H.M. Tan, T.C. Putti, S.W. Tang, C.W.Q. Ng, S.A. Buhari, E. Fang, M. Moothanchery, R. Bi, Biochemical "decoding" of breast ultrasound images with optoacoustic tomography fusion: first-in-human display of lipid and collagen signals on breast ultrasound, Photoacoustics 27 (2022) 100377.
[25] Gillies R.J., Kinahan P.E., Hricak H.J.R.: Radiomics: images are more than pictures, they are data. 2016, 278(2):563-577.
[26] Scapicchio C., Gabelloni M., Barucci A., Cioni D., Saba L., Neri EJLrm: A deep look into radiomics. 2021, 126(10):1296-1311.
[27] R.J. Gillies, P.E. Kinahan, H. Hricak, Radiomics: images are more than pictures, they are data, Radiology 278 (2) (2016) 563–577.
[28] Z.-L. Hong, S. Chen, X.-R. Peng, J.-W. Li, J.-C. Yang, S.-S. Wu, Nomograms for prediction of breast cancer in breast imaging reporting and data system (BI-RADS) ultrasound category 4 or 5 lesions: a single-center retrospective study based on radiomics features, Front. Oncol. 12 (2022) 894476.
[29] V. Romeo, R. Cuocolo, R. Apolito, A. Stanzione, A. Ventimiglia, A. Vitale, F. Verde, A. Accurso, M. Amitrano, L. Insabato, Clinical value of radiomics and machine learning in breast ultrasound: a multicenter study for differential diagnosis of benign and malignant lesions, Eur. Radiol. 31 (2021) 9511–9519.
[30] L. Zhong, L. Shi, L. Zhou, X. Liu, L. Gu, W. Bai, Development of a nomogram-based model combining intra- and peritumoral ultrasound radiomics with clinical features for differentiating benign from malignant in breast imaging reporting and data system category 3-5 nodules, Quant. Imaging Med. Surg. 13 (10) (2023) 6899–6910.
[31] Y. Guo, Y. Hu, M. Qiao, Y. Wang, J. Yu, J. Li, C. Chang, Radiomics analysis on ultrasound for prediction of biologic behavior in breast invasive ductal carcinoma, Clin. Breast Cancer 18 (3) (2018) e335–e344.
[32] Y. Zhu, Y. Dou, L. Qin, H. Wang, Z. Wen, Prediction of Ki-67 of invasive ductal breast cancer based on ultrasound radiomics nomogram, J. Ultrasound Med.: Off. J. Am. Inst. Ultrasound Med. 42 (3) (2023) 649–664.
[33] M. Jiang, C.-L. Li, X.-M. Luo, Z.-R. Chuan, R.-X. Chen, S.-C. Tang, W.-Z. Lv, X.-W. Cui, C.F. Dietrich, Radiomics model based on shear-wave elastography in the assessment of axillary lymph node status in early-stage breast cancer, Eur. Radiology 32 (4) (2022) 2313–2325.
[34] N. Braman, P. Prasanna, J. Whitney, S. Singh, N. Beig, M. Etesami, D.D.B. Bates, K. Gallagher, B.N. Bloch, M. Vulchi, et al., Association of peritumoral radiomics with tumor biology and pathologic response to preoperative targeted therapy for HER2 (ERBB2)-positive breast cancer, JAMA Netw. Open 2 (4) (2019) e192561.
[35] N.M. Braman, M. Etesami, P. Prasanna, C. Dubchuk, H. Gilmore, P. Tiwari, D. Plecha, A. Madabhushi, Intratumoral and peritumoral radiomics for the pretreatment prediction of pathological complete response to neoadjuvant chemotherapy based on breast DCE-MRI, Breast Cancer Res.: BCR 19 (1) (2017) 57.
[36] M.S. Bae, S.U. Shin, H.S. Ryu, W. Han, S.-A. Im, I.-A. Park, D.-Y. Noh, W.K. Moon, Pretreatment MR imaging features of triple-negative breast cancer: association with response to neoadjuvant chemotherapy and recurrence-free survival, Radiology 281 (2) (2016) 392–400.
[37] Z. Huang, K. Yang, H. Tian, H. Wu, S. Tang, C. Cui, S. Shi, Y. Jiang, J. Chen, J. Xu, et al., A validation of an entropy-based artificial intelligence for ultrasound data in breast tumors, BMC Med. Inform. Decis. Mak. 24 (1) (2024) 1.

Zhibin Huang, MD, is a resident of Ultrasound in The Second Clinical Medical College, Jinan University, China. He focuses on the clinical application of photoacoustic imaging and multi-modality imaging, especially the clinical diagnosis of diseases in breast and rheumatoid arthritics.

Sijie Mo, MD, is a resident of Ultrasound in The Second Clinical Medical College, Jinan University, China. Her fields of scientific interests: clinical application of photoacoustic imaging and multi-modality imaging, especially the clinical diagnosis of diseases in breast lesion.

Huaiyu Wu, MD, graduated from Jinan University, currently works at the Department of Ultrasound, Shenzhen People's Hospital. His research focuses on breast ultrasound, musculoskeletal ultrasound, artificial intelligence of ultrasound, photoacoustic imaging. Additionally, he has participated in a series of clinical trials in breast cancer imaging and rheumatoid arthritis imaging.

Xu Jinfeng, MD, Chief Physician, Professor of Second Clinical Medical College, Jinan University, Supervisor of Master's, Doctoral, and Postdoctoral candidates. Member of the Ultrasound Medicine Branch of the Chinese Medical Association and Deputy Leader of the Ninth Abdominal Group; Director of the Chinese Society of Ultrasound in Medicine Engineering, Deputy Chairman of the Abdominal Committee, and Deputy Chairman of the Committee on Superficial Organs and Peripheral Vessels; Vice Chairman of the Ultrasound Branch of the Guangdong Medical Association and Guangdong Medical Doctor Association; Chairman of the Ultrasound Branch of the Shenzhen Medical Association. Published more than 100 papers in national journals, over 90 papers in SCI-indexed journals, with the highest impact factor of **22.3**, and edited 5 professional books. Ranked in the top 10 national ultrasound medical scholars in 2022. Main research interests include abdominal and superficial organ ultrasound.

Luyao Zhou, MD, The Chief Physician of the Department of Ultrasound at Shenzhen Children's Hospital. The author has authored more than 60 publications, with over 40 of them as the first or corresponding author. These publications include 32 SCI papers, such as one in Nature Communications, two in the top-tier medical journal Radiology, one in the Journal of Internal Medicine, four in European Radiology, and three in AJR. The author has led two National Natural Science Foundation projects and two Guangdong Provincial Natural Science Foundation projects. The author has also received support from the Ke Lin New Star Talent Program at The First Affiliated Hospital of Sun Yat-sen University and the Young Teacher Basic Research Fund at Sun Yat-sen University.

Fajin Dong, MD, Chief Physician of the Ultrasound Department at Shenzhen People's Hospital, Supervisor of Master's Students. Specializes in abdominal, superficial, and musculoskeletal ultrasound diagnosis and intervention therapy. Published over 60 SCI papers as the first/corresponding author (representative papers published in internationally renowned journals such as Medical Image Analysis, Research, and Nature Communications), led and participated in numerous national, provincial, and municipal projects. Serves as a committee member of the Ultrasound Branch of the Chinese Medical Association's Superficial and Vascular Group; Member of the Musculoskeletal Ultrasound Special Committee of the Chinese Medical Doctor Association & Standing Committee Member of the Interventional Physicians Branch Pain Treatment Group; Member of the Musculoskeletal Special Committee of the Chinese Society of Ultrasound in Medicine Engineering, among others.